Performance Analysis of Resistive Superconducting Fault Current Limiter Using LN_2 and GHe Cooling

Roberto Oliveira, Xiaoze Pei, *Member, IEEE*, Emelie Nilsson, Jean-francois Rouquette, Jean Rivenc, Ludovic Ybanez, and Xianwu Zeng, *Member, IEEE*

***Abstract*—Large-scale electric aircraft is a disruptive technology to address the environmental impact of air travel. Fault current limitation is crucial to realise the safety and reliability of the electric aircraft, in particular for large-scale electric aircraft using DC distribution network. This paper investigates the behavior of the resistive SFCL under different cryogenic cooling systems including liquid nitrogen and helium gas circulation cooling systems for the electric aircraft DC distribution network. Electromagnetic and thermoelectric models were used to predict the characteristics of resistive SFCL. The simulation results demonstrate that it is promising to design resistive SFCL using liquid nitrogen cooling as well as helium gas circulation cooling systems, which offer flexibility for SFCL cryogenic cooling system for electric aircraft applications.**

***Index Terms*—ASCEND, electric aircraft, high-temperature superconductors, resistive superconducting fault current limiters.**

I. Introduction

LARGE-SCALE electric aircraft is a disruptive technology to address the environmental impact of air travel. Airbus UpNext has launched an advanced superconducting and cryogenic experimental powertrain demonstrator (ASCEND) project in 2021 to develop a superconducting electric aircraft propulsion system [1]. Fault current limitation is crucial to realise the safety and reliability of the electric aircraft under different fault conditions, in particular for large-scale electric aircraft using DC distribution network [2], [3], [4], [5]. The prospective fault current can be as high as tens of kA with a few milliseconds due to the closely coupled onboard electric network in the electric aircraft. The use of resistive superconducting fault current limiter (r-SFCL) has advantages over other types of SFCL, in particular its compact structure. Restive SFCLs are widely studied and there are a number of projects in operation and in development of SFCL using liquid nitrogen as cryogenic coolant [6].

The design of r-SFCL has to consider current limitation, selection of the superconducting tape, and SFCL coil temperature rise in addition to the recovery time after faults [7]. The use of computational models to predict the electromagnetic and thermal behavior of the SFCL has become a fundamental and key step in designing SFCL. There are different possible approaches to build the model in 1D, 2D and 3D [8], [9], [10]. Models can be built and evaluated by nodal methods that consider the conductance at each point in the circuit [11]. From there, the matrices are built with the corresponding parameters and the equations are solved. Another approach is the use of the finite element method to solve the equations at each intersection point between the geometric elements generated in the geometry of the evaluated device. For the electromagnetic analysis, the element has to be as small as possible whilst for thermoelectric analysis, it is sufficient to use regular shapes [12].

This paper presents the analysis of two different models where the 2D axisymmetric model to carry out the electromagnetic analysis of r-SFCL and the 2D model in xy-plane to analyse the thermoelectric behavior. The key contribution of the paper lies in that the behavior of SFCL under different cryogenic cooling system including liquid nitrogen (LN_2) at 65 K, helium gas (GHe) circulation at 40 K, 50 K and 65 K are investigated and compared.

II. Modelling

The computational model considers a superconducting tape ST-12-L manufactured by Shanghai Superconductor whose key parameters are presented in Table I. The model is highly flexible allowing investigation different topologies and boundary conditions using finite element software. The SFCL evaluated through this computational model is designed based on that the nominal DC voltage of 300 V for the electric aircraft.

This model considers a cylindrical cryostat where the heat transfer characteristics ($q_0 = h(T)(T_{ext} - T)$) for the coolant have the following co-relation ($h = N_u \cdot k_{coolant}/D$). The Nusselt number is influenced by the geometric characteristics of the environment ($Nu = 0.916 Re^{0.5} Pr^{1/3}$). The Reynolds ($Re = \rho u L/\mu$) and Prandtl ($Pr = C_p \mu/k$) numbers are considered initially.

TABLE I
SPECIFICATIONS OF THE SUPERCONDUCTOR

Description	Values
Manufacturer	Shanghai Sup.
Conductor type	ST-12-L
Width [mm]	12
Thickness of conductor [mm]	0.25
Substrate material	Hastelloy
Reinforced layer material	Stainless steel
Thickness of HTS layer [μm]	2
Thickness of substrate [μm]	50
Thickness of Stainless steel [μm]	80[a]
Thickness of silver layer [μm]	1.5[a]
Thickness of copper stabilizer [μm]	3.38
Minimum I_c @77 K [A]	500
Measured I_c of single tape @77 K [A]	510
Measured I_c of single tape @65 K [A]	1100
Resistance at 300 K [mΩ/m]	100

[a]One layer on each side.

A. Electromagnetic Model

The electromagnetic model used the $\boldsymbol{T}\boldsymbol{A}$-formulation (1)–(3) with the high-temperature superconductor (HTS) tapes being modelled in 2D axisymmetric. In this approach the state equations $\boldsymbol{T}$ and $\boldsymbol{A}$ can be defined by (3) and (4), respectively. Using Faraday's law (2) and (1) give the equation that governs the $\boldsymbol{T}$-formulation [13], [14].

$$\boldsymbol{J} = \nabla \times \boldsymbol{T} \tag{1}$$

$$\nabla \times \rho \boldsymbol{J} = -\frac{\partial \boldsymbol{B}}{\partial t} \tag{2}$$

$$\nabla \times \rho \nabla \times \boldsymbol{T} = -\frac{\partial \boldsymbol{B}}{\partial t} \tag{3}$$

Equation (4) expresses $\boldsymbol{A}$-formulation and governs the behavior in the region external to the superconducting layer. This one originates from of Ampere's Law (5) and the magnetic potential vector (6).

$$\nabla \times \nabla \times \boldsymbol{A} = \mu \boldsymbol{J} \tag{4}$$

$$\nabla \times \boldsymbol{B} = \mu \boldsymbol{J} \tag{5}$$

$$\boldsymbol{B} = \nabla \times \boldsymbol{A} \tag{6}$$

B. Thermoelectric Model

The thermoelectric model used the $\boldsymbol{H}$-formulation with HTS tapes being modelled in the 2D xy-plane. The current density and electric filed in type-II superconductors can be described by $E - J$ power law (7)–(8). The conductivity of the HTS layer is given by (9), considering flux creep in the $\boldsymbol{H}$-formulation (10)–(11).

$$\boldsymbol{E} = E_0 \left(\frac{|\boldsymbol{J}|}{J_c}\right)^n \frac{\boldsymbol{J}}{J_c} \tag{7}$$

$$J_c(T) = \begin{cases} J_{c0}\left(\dfrac{T_c - T}{T_c - T_0}\right) & \text{if } T < T_c \\ 0, & \text{if } T_c \leq T \end{cases} \tag{8}$$

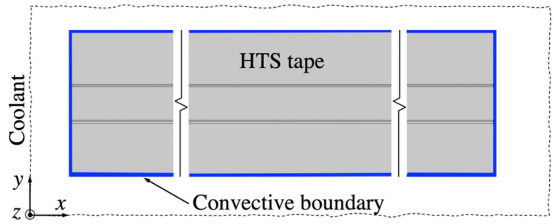

Fig. 1. Convective heat flux boundary.

$$\sigma_{HTS} = \frac{J_c(T)}{E_0}\left(\frac{\| E \|}{E_0}\right)^{\frac{1-n(T)}{n(T)}} \tag{9}$$

$$\nabla \times \boldsymbol{E} = -\mu_0 \mu_r \frac{\partial \boldsymbol{H}}{\partial t} \tag{10}$$

$$\nabla \times \boldsymbol{H} = \boldsymbol{J} \tag{11}$$

The 2D thermoelectric model considers an isothermal domain with a homogeneous temperature in space and which varies in time. The convective heat flux condition is assumed since the model represents the coolant adjacent to the device under analysis. The interface between the SFCL and the coolant is described by (12), with a heat transfer coefficient (h) given by the coolant. As the temperature variation is small in z-direction along the HTS tape in the model, the heat transfer in a 2D model is calculated using (13) [15], [16], [17]. Where n is the normal vector toward exterior (–), d_z is thickness of domain in the out-of-plane direction (m), k is thermal conductivity (W/mK), ρ_m is density (kg/m^3), C_p is specific heat capacity at constant pressure (J/kg K), q is conductive heat flux (W/m^2), h is heat transfer coefficient (W/m^{2}K) and Q is the heat source (W/m^3).

$$-\boldsymbol{n}_d \cdot (-d_z k \nabla T) = -h(T_{ext} - T) \tag{12}$$

$$-d_z \rho_m C_p \frac{\partial T}{\partial t} - \nabla \cdot \boldsymbol{q} = d_z Q + q_0 \tag{13}$$

The cryogenic coolant in which the SFCL is immersed is represented by a boundary condition between the tape and the coolant (blue line in Fig. 1). For LN_2 the heat transfer rate (h) is described by (14) [18] and for helium gas by (15) [19]–[20]. The characteristic of LN_2 considers the operation with a pressure of 1.5 bar and mass flow rate between 50–100 g/s. For helium gas circulation system, the pressure at 20 bar and mass flow rate between 5–10 g/s is considered. The electrical part is modelled by a nodal circuit with a voltage source of 300 V.

$$h_{LN_2}(\Delta T) = \begin{cases} 2170, & \text{if } \Delta T < 2, \\ (a_0 + a_1\Delta T + a_2\Delta T^2 & \\ +a_3\Delta T^3 + a_4\Delta T^4 & \\ +a_5\Delta T^5)/\Delta T, & \text{if } 2 < \Delta T < 26.5, \\ 100, & \text{if } \Delta T > 26.5. \end{cases} \tag{14}$$

$$h_{He}(\Delta T) = \begin{cases} 16000, & \text{if } \Delta T < 0.1, \\ 15100, & \text{if } 0.1 < \Delta T < 0.5 \\ 1400, & \text{if } \Delta T > 0.5. \end{cases} \tag{15}$$

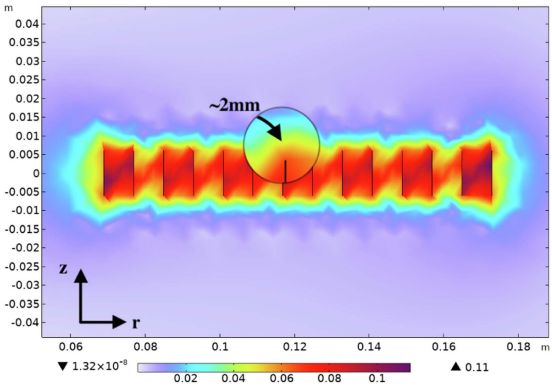

Fig. 2. Magnetic flux density [T] (for $I/I_c = 0.77$).

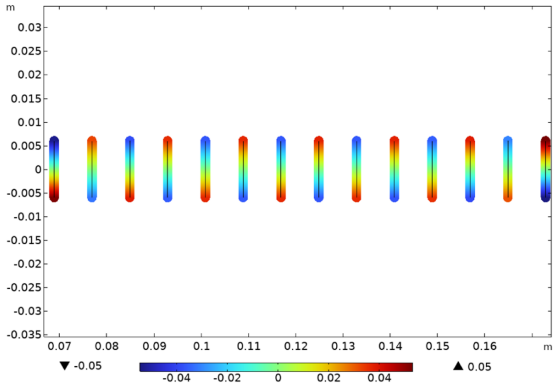

Fig. 4. Radial component of the magnetic flux density [T] for $I/I_c = 0.77$.

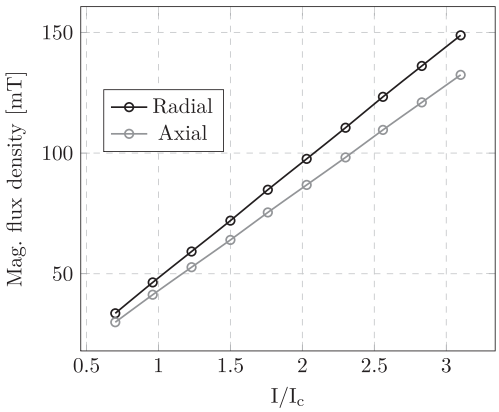

Fig. 3. Components of the magnetic flux density.

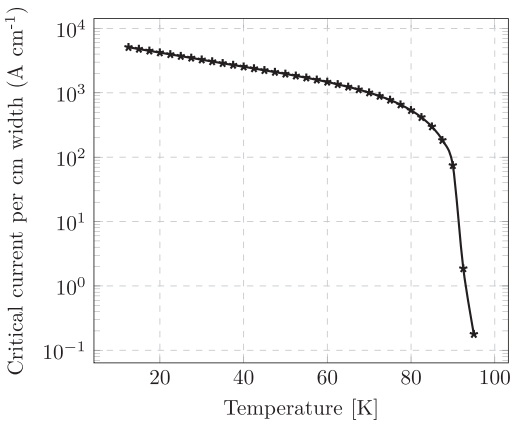

Fig. 5. Critical current of Shanghai Superconductor 2 G HTS tape at low field and high temperature.

Where $a_0 = 38147$, $a_1 = -28209$, $a_2 = 7232.8$, $a_3 = -494.38$, $a_4 = 13.25$, $a_5 = -0.12773$.

III. Electromagnetic Simulation Results

The electromagnetic model is 2D axisymmetric model along the z-axis and represents a non-inductive bifilar SFCL coil design. Only the superconducting layer ($2\,\mu$m thick and 12 mm wide, based on Table I) was considered. The SFCL coil has 14 turns with a total length of 10 m, inner diameter of 138 mm, outer diameter of 242 mm and inductance of $1.9\,\mu$H.

Fig. 2 presents the magnetic flux density for the SFCL under normal operation. This consists of two coils in parallel with a critical current of 1100 A at 65 K. For $I/I_c = 0.77$, the flux density has a maximum value of 0.11 T and the flux density between turns is 0.08 T. In the upper and lower limit region of the coil (≈ 2 mm in z-axis) the density is 0.03 T. During quench ($I/I_c = 2.3$) the maximum flux density value is 0.34 T, 0.23 T between turns and 0.18 T in the upper and lower limit region (z-axis). Fig. 3 shows the radial and axial component of the magnetic flux density under different currents. Fig. 4 shows the radial flux component for $I/I_c = 0.77$ on HTS tape and the cancellation of the flux due to the bifilar coil.

IV. Thermoelectric Simulation Results

Model developed and analysed in this section considered all the layers of the HTS tape described in Table I. SFCL with one coil and two coils connected in parallel are evaluated where the length of in each coil are 10 m. The critical current of the ST-12-L tape at 40 K, 50 K and 65 K were obtained from the available database, as shown in Fig. 5 [21].

A. LN_2 as Coolant

The total current and the distribution between the layers of the SFCL tape, during 10 ms fault, are shown in Fig. 6 where the grid voltage is $V_{grid} = 300$ V and the coil has two parallel tapes of 10 m each. LN_2 is used as a coolant at a pressure of 1.5 bar.

The total current in the system, resistance and temperature during the quench process are shown in Fig. 7. The temperature rise happens at a later time than the current due to the heat capacity. The temperature of the tape increases from 0.34 ms when the current already has an amplitude of 2 kA. The resistance is almost linear increase with the temperature from 5.4 ms when the resistance behavior is determined by the resistivity of the all other layers apart from HTS layer. Figs. 8 and 9 show the temperature distribution in each layer of SFCL HTS tape.

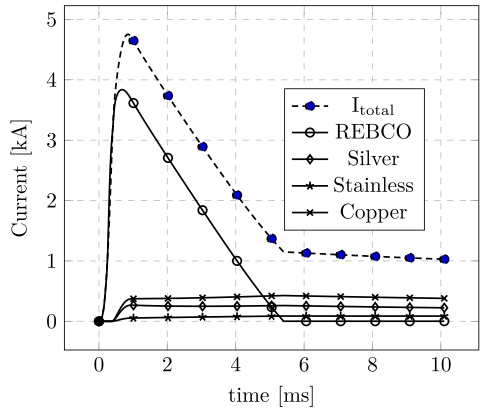

Fig. 6. Current in all layers where SFCL with 2 tapes in parallel of 10 m each in LN_2.

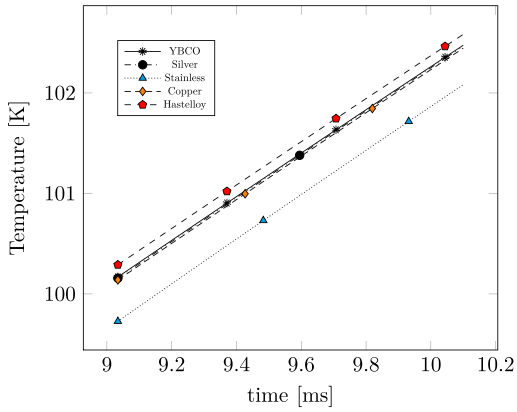

Fig. 9. Temperature distribution in each layer of SFCL HTS tape with 2 tapes in parallel of 10 m length each. LN_2 at an initial temperature of 65 K.

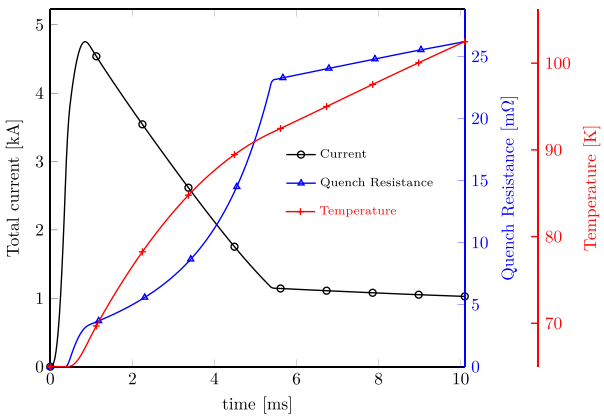

Fig. 7. Total current, Resistance and Temperature on SFCL coil cooled by LN_2 at 65 K where SFCL with 2 tapes in parallel of 10 m length each.

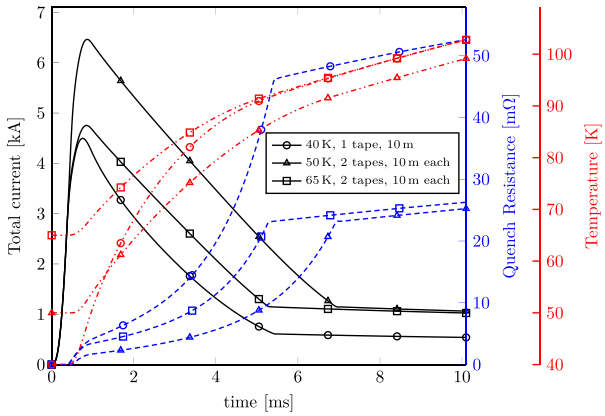

Fig. 10. Total current, Resistance and Temperature of SFCL coil cooled by He gas, where: **Solid** line present the total current, dashed line the quench resistance and dashed dotted line the temperature.

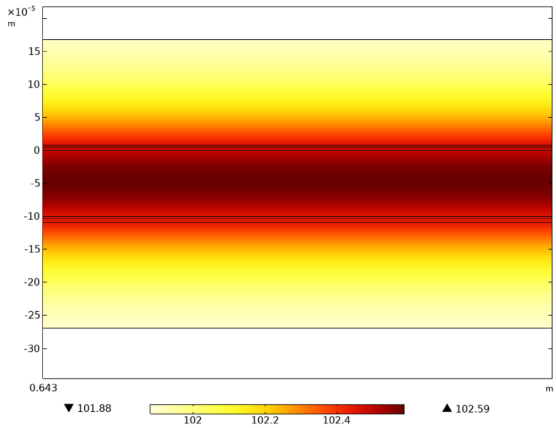

Fig. 8. Temperature distribution in the HTS tape layers at t=10 ms.

B. GHe as Coolant

The results presented in this section considers helium gas (GHe) at 40 K, 50 K and 65 K and the pressure of the system at 20 bar. Fig. 10 shows the total current in the system, resistance and temperature behavior during the quench process in the SFCL cooled by He gas. These three SFCL topologies with different cooling conditions satisfy the requirements. However, due to the resistance, current limitation time and temperature rise, each case must be evaluated for specific applications.

V. Discussion

This section presents the results, analysis and comparisons between the four cases investigated, and the summarised characteristics are described below:

- Case 1): SFCL with a 10 m long single tape. He gas at an initial temperature (T_0) of 40 K and $I_c = 2100$ A.
- Case 2): SFCL with two parallel tapes of 10 m long each. He gas at $T_0 = 50$ K and $I_c = 1600$ A for each tape.
- Case 3): SFCL with two tapes of 10 m in length each. He gas at $T_0 = 65$ K and $I_c = 1100$ A for each tape.
- Case 4): SFCL with two tapes of 10 m in length each. LN_2 at an initial temperature of 65 K and $I_c = 1100$ A for each tape.

Fig. 11 summarise the total limited current of the different SFCL topologies and cryogenic coolants (LN_2 and GHe). SFCL operating at an initial temperature of 65 K, considering an adiabatic system, can reach maximum temperatures from

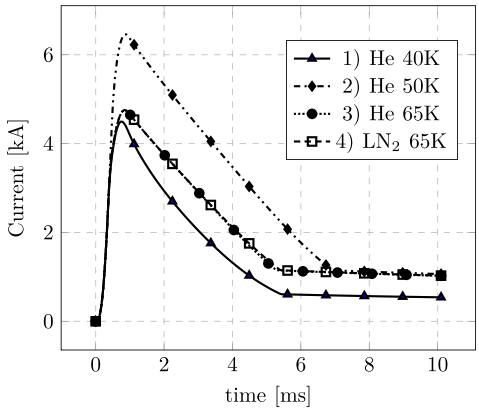

Fig. 11. Current limitation of the SFCL: 1) single tape, 10 m total length and 2), 3), 4) 2 tapes in parallel, 10 m each one.

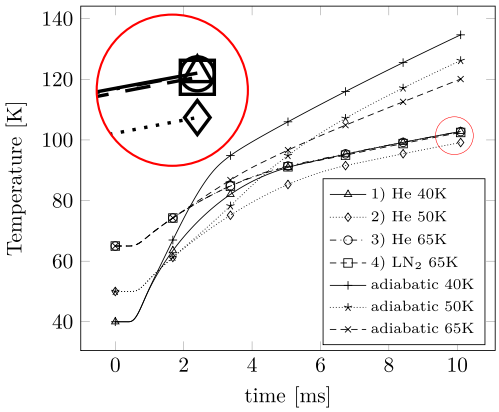

Fig. 12. Temperature of adiabatic and cooled system. 1) single tape, 10 m total length 2), 3) and 4) 2 tapes in parallel, 10 m each one.

137.49 K (2 coils in parallel and 10 m each). Under adiabatic conditions, the highest temperature is in stainless steel layers (top and bottom layers). All maximum temperature values in a cryogenic coolant-cooled conditions occur in the hastelloy layer. The temperature shown in Fig. 12 presents the temperature in the middle point of the HTS layer. Cases 1), 2), 3) and 4) have acceptable temperature responses and satisfy operating current and current limitation requirements when cooled with liquid nitrogen and helium gas.

For case 1) a single HTS tape is used due to the increase in the critical current at lower temperature. At 40 K the I_c is 2100 A, the current limitation would be too high if 2 taps in parallel is used. Case 1) has the value of the quench resistance of $R_q = 52.6\,\mathrm{m\Omega}$, which is higher than the same coil using two parallel tapes and therefore the final temperature after the fault period is slightly higher ($\Delta T = 6.01$ K). As described, case 1) and case 2) were cooled with GHe at different temperatures and the fault current in case 1) is 34.4% lower, despite the temperature being 3.57 K higher.

A comparison of the cryogenic cooling system conditions with GHe and LN_2, case 3) and case 4), presents that ΔT between them is very small and is shown in Fig. 12. And for an over-voltage operation ($V_{grid} = 350$ V), the maximum temperature would be 109.49 K at case 3), where, $\Delta T = 7$ K.

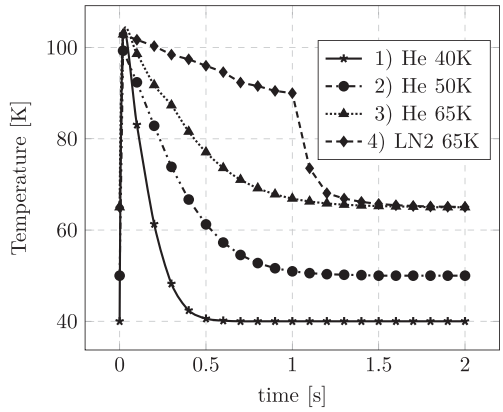

Fig. 13. Recovery response of the SFCL: 1) single tape, 10 m in length and 2), 3), 4) 2 tapes in parallel, 10 m each one.

The maximum temperature of SFCL for Cases 1), 2) and 3) can reach is 102.89 K with $T_0 = 65$ K and the lowest maximum temperature of 99.31 K with $T_0 = 50$ K and $R_q = 25.2\,\mathrm{m\Omega}$. In case 4) the results show that the maximum temperature would reach 102.59 K with quench resistance of $R_q = 26.2\,\mathrm{m\Omega}$.

The recovery time in Fig. 13 shows that the use of GHe (case 1) achives a faster recovery in the temperature of the SFCL when compared to LN_2 operating at 65 K (case 4). When the coolant is LN_2, there is a sharp reduction in temperature when reaching the nitrogen phase change. The recovery in the GHe circulation system at 40 K can be up to three times faster than using LN_2 at 65 K.

VI. Conclusion

Resistive SFCLs have been successfully demonstrated and tested in LN_2 at 77 K and sub-cooled LN_2 at 65 K. However, there is limited study if resistive SFCLs can operate using helium gas circulation system. This paper investigates resistive SFCLs under adiabatic condition, liquid nitrogen of 65 K and helium gas of 40 K, 50 K and 65 K. The simulation results show that the operation of the SFCL with LN_2 at 65 K and GHe at 40 K, 50 K and 65 K can provide an acceptable limited fault current and satisfy the temperature requirements while keeping the losses of the cryogenic system at reasonable levels. The temperature rise of the HTS tape using LN_2 and GHe cryogenic cooling system are well below the maximum temperature allowed. All four cooling cases using liquid nitrogen and helium gas are useful and can be viable solutions for resistive SFCLs using HTS tapes used, which offers flexibility in designing the cryogenic cooling system for electric aircraft applications.

References

[1] L. Ybanez et al., "ASCEND: The first step towards cryogenic electric propulsion," *IOP Conf. Series: Mater. Sci. Eng.*, vol. 1241, no. 1, 2022, Art. no. 012034, doi: 10.1088/1757-899x/1241/1/012034.

[2] P. J. Masson, D. S. Soban, E. Upton, J. E. Pienkos, and C. A. Luongo, "HTS motors in aircraft propulsion: Design considerations," *IEEE Trans. Appl. Supercond.*, vol. 15, no. 2, pp. 2218–2221, Jun. 2005, doi: 10.1109/TASC.2005.849616.

[3] F. Berg, J. Palmer, P. Miller, and G. Dodds, "HTS system and component targets for a distributed aircraft propulsion system," *IEEE Trans. Appl. Supercond.*, vol. 27, no. 4, Jun. 2017, Art. no. 3600307, doi: 10.1109/TASC.2017.2652319.

[4] S. Imparato et al., "Experimental evaluation of AC losses of a DC restive SFCL prototype," *IEEE Trans. Appl. Supercond.*, vol. 20, no. 3, pp. 1199–1202, Jun. 2010, doi: 10.1109/TASC.2010.2043726.

[5] J. Xi, X. Pei, W. Song, B. Xiang, Z. Liu, and X. Zeng, "Experimental tests of DC SFCL under low impedance and high impedance fault conditions," *IEEE Trans. Appl. Supercond.*, vol. 31, no. 5, Aug. 2021, Art. no. 5601205, doi: 10.1109/TASC.2021.3065886.

[6] P. Seidel, *Applied Superconductivity: Handbook on Devices and Applications*. Hoboken, NJ, USA: Wiley, 2015.

[7] P. Tixador, *Superconducting Fault Current Limiter: Innovation for the Electric Grids*. Vol. 3. Singapore: World Scientific, 2018.

[8] F. Grilli et al., "Finite-element method modeling of superconductors: From 2-D to 3-D," *IEEE Trans. Appl. Supercond.*, vol. 15, no. 1, pp. 17–25, Mar. 2005, doi: 10.1109/TASC.2004.839774.

[9] G. dos Santos, F. G. R. Martins, F. Sass, G. G. Sotelo, A. Morandi, and F. Grilli, "A 3-D finite-element method approach for analyzing different short circuit types in a saturated iron core fault current limiter," *IEEE Trans. Appl. Supercond.*, vol. 32, no. 3, Apr. 2022, Art. no. 5600713, doi: 10.1109/TASC.2022.3142047.

[10] B. Shen, F. Grilli, and T. Coombs, "Overview of H-formulation: A versatile tool for modeling electromagnetics in high-temperature superconductor applications," *IEEE Access*, vol. 8, pp. 100403–100414, 2020, doi: 10.1109/ACCESS.2020.2996177.

[11] W. T. Batista de Sousa, D. Kottonau, and M. Noe, "Transient simulation and recovery time of a three-phase concentric HTS cable," *IEEE Trans. Appl. Supercond.*, vol. 29, no. 5, Aug. 2019, Art. no. 5401705, doi: 10.1109/TASC.2019.2900937.

[12] F. Grilli, E. Pardo, A. Stenvall, D. N. Nguyen, W. Yuan, and F. Gömöry, "Computation of losses in HTS under the action of varying magnetic fields and currents," *IEEE Trans. Appl. Supercond.*, vol. 24, no. 1, Feb. 2014, Art. no. 8200433, doi: 10.1109/TASC.2013.2259827.

[13] H. Zhang, M. Zhang, and W. Yuan, "An efficient 3D finite element method model based on the T–A formulation for superconducting coated conductors," *Superconductor Sci. Technol.*, vol. 30, no. 2, 2016, Art. no. 024005.

[14] E. Berrospe-Juarez, "Electromagnetic modeling of large-scale high-temperature superconductor systems," 2020, *arXiv:2006.02033*.

[15] C. Lacroix and F. Sirois, "Concept of a current flow diverter for accelerating the normal zone propagation velocity in 2 G HTS coated conductors," *Superconductor Sci. Technol.*, vol. 27, no. 3, 2014, Art. no. 035003.

[16] N. Riva, F. Grilli, and B. Dutoit, "Superconductors for power applications: An executable and web application to learn about resistive fault current limiters," *Eur. J. Phys.*, vol. 42, no. 4, 2021, Art. no. 045802.

[17] J. Ma, J. Geng, W. Chan, J. Schwartz, and T. Coombs, "A temperature-dependent multilayer model for direct current carrying HTS coated-conductors under perpendicular AC magnetic fields," *Supercond. Sci. Technol.*, 33, no. 4, 2020, Art. no. 045007.

[18] W. G. Fastowski, J. W. Petrowski, and A. E. Rowinski, *Kryotechnik*. Berlin, Germany: Akademie-Verlag, 1970.

[19] M. D. Donne and G. P. Tartaglia, Heat transfer for turbulent flow of helium or hydrogen in a tube at high temperatures: evaluation with the method of Petukhov. No KFK–3593. Kernforschungszentrum Karlsruhe GmbH (Germany), 1983.

[20] R. D. McCarty, "Thermophysical properties of Helium-4 from 2 to 1500 k. with pressures to 1000 atmospheres," vol. 631. *US Government Printing Office*, 1972.

[21] Victoria University of Wellington, "Critical current per cm width." Accessed: Oct. 7, 2022. [Online]. Available: https://htsdb.wimbush.eu/dataset/19185092